Ocean Engineering 257 (2022) 111600

Contents lists available at ScienceDirect

Ocean Engineering

journal homepage: www.elsevier.com/locate/oceaneng

Bidirectional Whitham type equations for internal waves with variable topography

Chunxin Yuan [a], Zhan Wang [b,c,d,*]

[a] School of Mathematical Sciences, Ocean University of China, Songling 238 Road, Qingdao, 266100, PR China
[b] Institute of Mechanics, Chinese Academy of Sciences, Beijing, 100190, PR China
[c] School of Engineering Science, University of Chinese Academy of Sciences, Beijing, 100049, PR China
[d] School of Future Technology, University of Chinese Academy of Sciences, Beijing, 100049, PR China

ARTICLE INFO

Keywords:
Whitham type equations
Bidirectional propagation
Full dispersion
Internal waves

ABSTRACT

In the context of oceanic internal gravity waves, one of the most widely-used theories on examining wave dynamics and interpreting observational data is the Korteweg–de Vries (KdV) equation. Nonetheless, the characters of unidirectional propagation and unbounded phase and group velocities restrict its application to some general cases (Benjamin et al., 1972). Thus, using the Dirichlet–Neumann operator with the rigid-lid approximation, we derive both bidirectional and unidirectional Whitham type equations in the Hamiltonian framework, which retain the full linear dispersion relation of the Euler equations. The effect of topography is also incorporated in modeling due to its practical relevance, although the invoked scaling plausibly excludes the accommodation of a significant bottom variation. There are no analytic solutions of internal solitary waves explicitly given in the newly proposed equations, even though these equations possess a concise form. Therefore, a modified Petviashvili iteration method is implemented to obtain the numerical solutions to circumvent this difficulty. Facilitated by these techniques, several numerical experiments are investigated and compared among different models: the KdV equation, the Whitham type equations, and the primitive equations. The discrepancies and similarities between the various models jointly indicate the advantage of full dispersion and bidirectional propagation and, thus, the effectiveness of the Whitham type equations.

1. Introduction

Internal wave is a ubiquitous phenomenon in the coastal ocean (Ramp et al., 2004; Shroyer et al., 2010). As the name implies, the largest amplitude of internal waves emerges in the interior, usually near the pycnocline, and decays along with both upward and downward directions. Internal waves play an important role in the vertical transport of momentum, heat, and mass, which help maintain the overturning circulation to impact the climate system further. In addition, internal waves are important for submarine navigation and detection; for instance, the disaster of the Indonesian submarine in the Bali Sea that occurred in April 2021 is plausibly attributed to internal waves, see Barker (2021).

Generally, considering the typical background environment, oceanic internal gravity waves with an amplitude of $\mathcal{O}(100)$ m merely induce surface waves with an amplitude of $\mathcal{O}(1)$ cm. This almost invisible feature on the surface makes detection difficult. Nonetheless, as the restoring force of buoyancy is essentially weak, internal waves can possess large amplitudes and strong currents even induced by a small disturbance. Therefore, these waves pose potential threats on oil platforms, and indeed, it has been recorded that, after a passage of internal waves in the Andaman Sea, the oil drilling platform was rotated 90° and pushed 30.48 m away from its installation site. Similarly, in the South China Sea, a mooring oil tank swung 110° in less than 5 minutes when it encountered internal waves; see Cai and Gan (2001) for more ocean engineering accidents due to internal waves.

Internal waves possess different spatial (from few meters to one hundred kilometers) and temporal (from few minutes to dozens of hours) scales and internal solitary waves (also called internal solitons), usually with high nonlinearity and large amplitude, have attracted much attention. In the 1960s, by virtue of the development of modern instruments for *in-situ* observation, the quantitative measurement of internal waves emerged. One of the earliest clear observational evidence of internal solitary waves was in the Strait of Gibraltar (Ziegenbein, 1969, 1970). These waves were also recorded by Osborne and Burch (1980), and more importantly, they provide a paradigm for implementing

* Corresponding author at: Institute of Mechanics, Chinese Academy of Sciences, Beijing, 100190, PR China.
E-mail address: zwang@imech.ac.cn (Z. Wang).

https://doi.org/10.1016/j.oceaneng.2022.111600
Received 12 February 2022; Received in revised form 16 April 2022; Accepted 20 May 2022
Available online 6 June 2022

the Korteweg–de Vries (KdV) equation to describe observational internal solitary waves. The celebrated KdV equation, which had already achieved great success in the fields of nonlinear waves (hydrodynamics, plasma, etc.), prospered in this new aspect owing in large part to its good delineation of observations (see Ostrovsky and Stepanyants, 2005; Klymak et al., 2006; Li et al., 2015; Grimshaw et al., 2016 for instance) and, as well, its succinct form. Inspired by these, several variants of the KdV equation were proposed. Of note is the Gardner equation for large-amplitude internal waves by introducing the cubic nonlinearity (Djordjevic and Redekopp, 1978; Grimshaw et al., 2002), the Ostrovsky equation by involving a nonlocal term reflecting the Earth's rotation (Ostrovsky, 1978), and the variable-coefficient KdV equation by incorporating the effects of background shear, continuous stratification, and slowly varying topography (Grimshaw, 1981; Zhou and Grimshaw, 1989). Theoretically, the KdV type equations shall only be applied to the shallow-water situation. In contrast, the Intermediate Long Wave (ILW) equation proposed by Joseph (1977) and Kubota et al. (1978) accounts for intermediate depth, and the Benjamin–Ono (BO) equation is adopted for infinitely deep fluids (Benjamin, 1966; Ono, 1975). On the other hand, owing to the disparity of the internal and surface waves' length scales, their interactions are of interest; see Craig et al. (2012) and Jiang et al. (2019) for example.

Although the equations mentioned above are widely implemented on internal solitary waves, one of their theoretical premises – the assumption of weak nonlinearity – limits their applications, especially when large-amplitude waves are involved. Miyata (1988) and Choi and Camassa (1999) derived the Miyata–Choi–Camassa (MCC) equations with full nonlinearity and weak dispersion to circumvent this shortcoming. Recently, strongly nonlinear models for three-layer flows were also developed to study the mode-2 internal waves by Barros et al. (2020) and Wang et al. (2022). Nonetheless, a more accurate way to investigate internal solitary waves is in the framework of the Dubreil–Jacotin–Long (DJL) equation (Benjamin, 1966; Tung et al., 1982), which amounts to the full set of stratified Euler equations. However, the trade-off is that the DJL equation is time-independent, and it cannot delineate wave evolution scenarios.

In recent years, benefited from the rapid advance of satellite techniques, the accumulation of many remote sensing images has facilitated the investigations on three-dimensional (3D) internal solitary waves. One of the most prominent theoretical models is the Kadomtsev–Petviashvili (KP) equation (Kadomtsev and Petviashvili, 1970), which is generally a variant of the KdV equation. A few pieces of research, such as Cai and Xie (2010) and Yuan et al. (2018), invoked the KP equation to study internal solitary waves propagating over two-dimensional (2D) topographies under a two-layer or a continuously stratified fluid. Nevertheless, the KP equation is unidirectional, and it only suits the case in which variations in the y-direction are one order smaller than those in the x-direction. Thus Yuan et al. (2020) derived a bidirectional isotropic model for internal waves, termed the modified Benney–Luke equation indicating the heritage of the classic Benney–Luke equation for free-surface water waves.

Nowadays, with the development of computational fluid dynamics and the availability of powerful supercomputers, comprehensive oceanic models possessing the ability to resolve a large number of multi-scale dynamical processes simultaneously are being increasingly used to simulate internal waves; see the reviews by Simmons et al. (2011) and Guo and Chen (2014). These models are usually based on the primitive Navier–Stokes equations, which are so complicated that using a very fine resolution in large 3D simulations is generally impossible due to the limitation of supercomputers. In practice, parameterization schemes are implemented to represent the contributions of these unresolved small-scale phenomena, which, however, requires a deep insight into the dynamical processes. Nevertheless, the full Navier–Stokes equations with complicated free boundary conditions are generally inconvenient for exploring the physical properties of a specific phenomenon; still, theoretical models can come into play in this case.

The rest of the paper is structured as follows. To overcome the shortcomings of the widely-used KdV equation (unidirectional propagation and no lower bound of the phase velocity at large wavenumber), we derive the Whitham type equations that retain the full dispersion relation in Section 2. Since conducting a deep analysis of the proposed equations is too mathematically involved and beyond the scope of the paper, we resort to detailed numerical simulations in Section 3, together with the illustrations of numerical results. Finally, we conclude and discuss in Section 4.

2. Derivation

2.1. Mathematical formulation

We consider two two-dimensional incompressible, inviscid, and homogeneous fluids bounded together, with the lighter fluid lying on top of the heavier one. Two fluids are immiscible and separated by a sharp interface $z = \eta(x,t)$, where x is the direction of wave propagation, and the z-axis points upwards with $z = 0$ the undisturbed interface. A sketch of the system is shown in Fig. 1. The upper layer is bounded above by a flat rigid lid $z = h^+$, while the lower layer is bounded below by a bottom topography $z = -h^- + b(x)$. It is noted that the justification of the rigid-lid approximation on the two-layer fluid has been provided by Duchene (2014). The subscripts + and - refer to fluid properties associated with the upper and lower layers, respectively. The fluid density in each layer is supposed to be constant, designated by $\rho^\pm$, and the system is in a stable density configuration, namely $\rho^+ < \rho^-$. The motion of each fluid is assumed to be irrotational; thus, we can introduce velocity potentials $\phi^\pm$, which satisfy the Laplace equation in the corresponding layers, namely

$$\phi^-_{xx} + \phi^-_{zz} = 0\,, \quad \text{for } -h^- + b(x) < z < \eta(x,t)\,,$$
$$\phi^+_{xx} + \phi^+_{zz} = 0\,, \quad \text{for } \eta(x,t) < z < h^+\,.$$

On the interface $z = \eta(x,t)$, the nonlinear kinematic and dynamic boundary conditions read

$$\eta_t = \phi^-_z - \eta_x\phi^-_x = \phi^+_z - \eta_x\phi^+_x\,, \tag{1}$$
$$0 = \rho^-\left(\phi^-_t + g\eta + \frac{1}{2}|\nabla\phi^-|^2\right) - \rho^+\left(\phi^+_t + g\eta + \frac{1}{2}|\nabla\phi^+|^2\right)\,, \tag{2}$$

where g is the acceleration due to gravity. The kinematic boundary condition (1) implies that the normal velocity is continuous across the interface

$$\left(\phi^-_x, \phi^-_z\right)^\top \cdot \mathbf{n} = \left(\phi^+_x, \phi^+_z\right)^\top \cdot \mathbf{n}\,, \tag{3}$$

where $\mathbf{n} = (-\eta_x, 1)^\top / \sqrt{1+\eta_x^2}$ is the unit normal vector on the interface pointing upwards. Finally, the impermeability boundary conditions,

$$\phi^+_z = 0\,, \quad \text{at } z = h^+\,, \tag{4}$$
$$\phi^-_z - b_x\phi^-_x = 0\,, \quad \text{at } z = -h^- + b(x)\,, \tag{5}$$

complete the whole system. For $b = 0$, linearizing the above governing equations and boundary conditions and then solving for wavy solutions, one obtains the dispersion relation between wavenumber k and frequency ω:

$$\omega^2 = \frac{g(\rho^- - \rho^+)|k|}{\rho^-\coth(|k|h^-) + \rho^+\coth(|k|h^+)}\,. \tag{6}$$

2.2. Hamiltonian formulation

Benjamin and Bridges (1997) proved that the interfacial wave system has a Hamiltonian structure. The canonical variables are the difference between interfacial velocity potentials $\xi = \rho^-\phi^-(x,\eta,t) -$

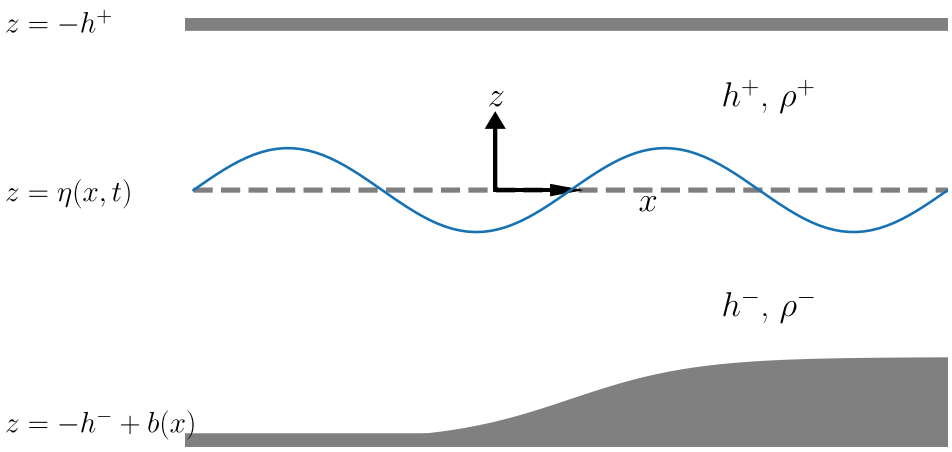

Fig. 1. Sketch of the problem and coordinate system.

$\rho^+\phi^+(x,\eta,t)$ and the interface displacement η. The Hamiltonian functional is the sum of kinetic and potential energies, *i.e.*,

$$\mathcal{H}[\eta,\xi] = \frac{\rho^-}{2}\int_{\mathbb{R}}\int_{-h^-+b}^{\eta}|\nabla\phi^-|^2\mathrm{d}z\mathrm{d}x + \frac{\rho^+}{2}\int_{\mathbb{R}}\int_{\eta}^{h^+}|\nabla\phi^+|^2\mathrm{d}z\mathrm{d}x + \frac{(\rho^- - \rho^+)g}{2}\int_{\mathbb{R}}\eta^2\mathrm{d}x\,, \tag{7}$$

and the canonical variables satisfy Hamilton's equations

$$\eta_t = \frac{\delta\mathcal{H}}{\delta\xi}\,, \qquad \xi_t = -\frac{\delta\mathcal{H}}{\delta\eta}\,. \tag{8}$$

The Dirichlet–Neumann operator (DNO) is essential for investigating free boundary problems in potential theory. We first define the velocity potentials at the interface as

$$\xi^-(x,t) = \phi^-(x,\eta(x,t),t)\,, \qquad \xi^+(x,t) = \phi^+(x,\eta(x,t),t).$$

Following Craig and Sulem (1993), we introduce the Dirichlet-Neumann operators (DNOs)

$$G^+\left(\eta,h^+\right)\xi^+ = \left[\eta_x\phi_x^+ - \phi_z^+\right]_{z=\eta} = \nabla\phi^+\cdot(-\mathbf{n})\sqrt{1+\eta_x^2}\,, \tag{9}$$

$$G^-\left(\eta,h^-,b\right)\xi^- = \left[\phi_z^- - \eta_x\phi_x^-\right]_{z=\eta} = \nabla\phi^-\cdot\mathbf{n}\sqrt{1+\eta_x^2}\,. \tag{10}$$

The DNOs essentially map the Dirichlet boundary conditions to normal derivatives by solving Laplace's equations. We suppress the dependency of DNOs on $h^\pm$, b, and η in subsequent analyses for the simplicity of notations. Then the kinematic boundary condition at the interface can be rewritten as a compact form

$$\eta_t = G^-\xi^- = -G^+\xi^+\,, \tag{11}$$

which gives the relations between ξ and $\xi^\pm$:

$$G^+\xi = (\rho^-G^+ + \rho^+G^-)\xi^- \Longrightarrow \xi^- = (\rho^-G^+ + \rho^+G^-)^{-1}G^+\xi\,, \tag{12}$$

$$G^-\xi = -(\rho^-G^+ + \rho^+G^-)\xi^+ \Longrightarrow \xi^+ = -(\rho^-G^+ + \rho^+G^-)^{-1}G^-\xi\,. \tag{13}$$

Based on the DNOs, the Hamiltonian can be rewritten as

$$\mathcal{H}[\eta,\xi] = \frac{1}{2}\int_{\mathbb{R}}\xi G^-\left(\rho^-G^+ + \rho^+G^-\right)^{-1}G^+\xi\mathrm{d}x + \frac{(\rho^- - \rho^+)g}{2}\int_{\mathbb{R}}\eta^2\mathrm{d}x\,. \tag{14}$$

2.3. Expansions of DNOs

Meyer (1985) proved that the DNO is an analytic function if the L^1-norm and Lipschitz-norm of η are smaller than a certain constant. It then follows that DNOs can be naturally written in the form of convergent Taylor expansion in η. A recursive formula for the expansion of the DNO in the two-dimensional water-wave problem with flat bottom was initially obtained by Craig and Sulem (1993), and later on generalization to include variable bottom topography by Craig et al. (2005). Recently, Ablowitz et al. (2006) proposed an explicit non-local formulation for the classical water-wave problem in two and three dimensions. It was also generalized to include the bottom topography by Fokas and Nachbin (2012) and Andrade and Nachbin (2018).

In the present paper, we derive the Taylor expansion of DNOs by virtue of the Ablowitz–Fokas–Musslimani formulation in the spirit of Whitham (1974), namely to retain the full linear dispersion relation for weakly nonlinear long-wave models. First of all, it is straightforward to verify that the following identity

$$\left(\phi_z^\pm\psi_x + \phi_x^\pm\psi_z\right)_x + \left(\phi_z^\pm\psi_z - \phi_x^\pm\psi_x\right)_z = 0 \tag{15}$$

holds for an arbitrary harmonic function ψ. Applying the divergent theorem to Eq. (15) in the lower layer yields

$$0 = \int\left[b_x\left(\phi_z^-\psi_x + \phi_x^-\psi_z\right) - \left(\phi_z^-\psi_z - \phi_x^-\psi_x\right)\right]_{z=-h^-+b}\mathrm{d}x + \int\left[-\eta_x\left(\phi_z^-\psi_x + \phi_x^-\psi_z\right) + \left(\phi_z^-\psi_z - \phi_x^-\psi_x\right)\right]_{z=\eta}\mathrm{d}x\,. \tag{16}$$

Substituting $\psi = e^{\mathrm{i}kx+|k|z}$ into Eq. (16) gives

$$0 = \int e^{\mathrm{i}kx+|k|(\eta+h^-)}\left[|k|\eta_t - \mathrm{i}k\xi_x^-\right]\mathrm{d}x + \int e^{\mathrm{i}kx+|k|b}\left[\mathrm{i}k\Phi_x^b\right]\mathrm{d}x\,, \tag{17}$$

where Eqs. (1) and (5), as well as the definition of ξ^-, have been used, and $\Phi^b = \phi^-(x,-h^-+b,t)$ is the velocity potential at the bottom. Since $e^{\mathrm{i}kx-|k|z}$ is also a solution to the Laplace equation, one also obtains

$$0 = \int e^{\mathrm{i}kx-|k|(\eta+h^-)}\left[-|k|\eta_t - \mathrm{i}k\xi_x^-\right]\mathrm{d}x + \int e^{\mathrm{i}kx-|k|b}\left[\mathrm{i}k\Phi_x^b\right]\mathrm{d}x\,. \tag{18}$$

Adding and subtracting (17) and (18) yield

$$0 = \int e^{\mathrm{i}kx}\left[|k|\sinh(|k|(\eta+h^-))\eta_t - \mathrm{i}k\xi_x^-\cosh(|k|(\eta+h^-)) + \mathrm{i}k\Phi_x^b\cosh(|k|b)\right]\mathrm{d}x \tag{19}$$

and

$$0 = \int e^{\mathrm{i}kx}\left[\cosh(|k|(\eta+h^-))\eta_t - \mathrm{i}k\xi_x^-\frac{\sinh(|k|(\eta+h^-))}{|k|} + \mathrm{i}k\Phi_x^b\frac{\sinh(|k|b)}{|k|}\right]\mathrm{d}x\,. \tag{20}$$

In the same vein, one can obtain the global relation for the upper layer:

$$0 = \int e^{\mathrm{i}kx}\left[\cosh(|k|(h^+-\eta))\eta_t + \mathrm{i}k\xi_x^+\frac{\sinh(|k|(h^+-\eta))}{|k|}\right]\mathrm{d}x\,. \tag{21}$$

To derive weakly nonlinear models in the shallow-water regime, we assume a small-amplitude motion in addition to the long-wave assumption. Supposing that the typical bottom amplitude is similar to the interface, the Boussinesq scaling is used:

$$x\sim L\,,\quad z\sim h^-\,,\quad \eta,b\sim a\,,\quad t\sim\frac{L}{\sqrt{gh^-(1-R)}}\,,\quad \xi^\pm\,,$$
$$\boldsymbol{\Phi}^b\sim\frac{aL\sqrt{g(1-R)}}{\sqrt{h^-}}\,, \tag{22}$$

where a is the typical amplitude, and L is the typical wavelength. Small parameters $\epsilon=\frac{a}{h^-}$ and $\mu=\frac{h^-}{L}$ are introduced to measure the nonlinearity and dispersion, respectively, and $\sigma=\frac{h^+}{h^-}$ is $\mathcal{O}(1)$ hereafter. After non-dimensionalization, the global relations (19)–(21) read

$$0=\int e^{\mathrm{i}kx}\left[\mu|k|\sinh(\mu|k|(1+\epsilon\eta))\eta_t-\mathrm{i}k\xi_x^-\cosh(\mu|k|(1+\epsilon\eta))\right.$$
$$\left.+\mathrm{i}k\boldsymbol{\Phi}_x^b\cosh(\epsilon\mu|k|b)\right]\mathrm{d}x\,, \tag{23}$$

$$0=\int e^{\mathrm{i}kx}\left[\cosh(\mu|k|(1+\epsilon\eta))\eta_t-\mathrm{i}k\xi_x^-\frac{\sinh(\mu|k|(1+\epsilon\eta))}{\mu|k|}\right.$$
$$\left.+\mathrm{i}k\boldsymbol{\Phi}_x^b\frac{\sinh(\epsilon\mu|k|b)}{\mu|k|}\right]\mathrm{d}x\,, \tag{24}$$

and

$$0=\int e^{\mathrm{i}kx}\left[\cosh(\mu|k|(\sigma-\epsilon\eta))\eta_t+\mathrm{i}k\xi_x^+\frac{\sinh(\mu|k|(\sigma-\epsilon\eta))}{\mu|k|}\right]\mathrm{d}x\,. \tag{25}$$

Taking the Taylor series expansions of the global relations around $\epsilon=0$ and retaining terms valid up to $O(\epsilon)$, one obtains

$$0=\int e^{\mathrm{i}kx}\left\{\mu|k|\left[\sinh(\mu|k|)+\epsilon\mu|k|\cosh(\mu|k|)\eta\right]\eta_t-\mathrm{i}k\xi_x^-\left[\cosh(\mu|k|)\right.\right.$$
$$\left.\left.+\epsilon\mu|k|\sinh(\mu|k|)\eta\right]+\mathrm{i}k\boldsymbol{\Phi}_x^b\right\}\mathrm{d}x\,, \tag{26}$$

$$0=\int e^{\mathrm{i}kx}\left\{\left[\cosh(\mu|k|)+\epsilon\mu|k|\sinh(\mu|k|)\eta\right]\eta_t\right.$$
$$\left.-\mathrm{i}k\xi_x^-\left[\frac{\sinh(\mu|k|)}{\mu|k|}+\epsilon\cosh(\mu|k|)\eta\right]+\mathrm{i}k\boldsymbol{\Phi}_x^b(\epsilon b)\right\}\mathrm{d}x\,, \tag{27}$$

$$0=\int e^{\mathrm{i}kx}\left\{\left[\cosh(\mu|k|\sigma)-\epsilon\mu|k|\sinh(\mu|k|\sigma)\eta\right]\eta_t\right.$$
$$\left.+\mathrm{i}k\xi_x^+\left[\frac{\sinh(\mu|k|\sigma)}{\mu|k|}-\epsilon\cosh(\mu|k|\sigma)\eta\right]\right\}\mathrm{d}x\,. \tag{28}$$

Upon noting $\mathrm{i}k\sim-\partial_x$ and $k^2\sim-\partial_{xx}$, the inverse Fourier transforms of (26)–(28) give

$$0=\mu D\tanh(\mu D)\eta_t-\epsilon\mu^2(\eta\eta_t)_{xx}+\xi_{xx}^-+\epsilon\left[\mu D\tanh(\mu D)\eta\xi_x^-\right]_x-\frac{\boldsymbol{\Phi}_{xx}^b}{\cosh(\mu D)}\,, \tag{29}$$

$$0=\left[1+\epsilon\mu D\tanh(\mu D)\eta\right]\eta_t+\frac{\tanh(\mu D)}{\mu D}\xi_{xx}^-+\epsilon(\eta\xi_x^-)_x-\frac{\epsilon\left(b\boldsymbol{\Phi}_x^b\right)_x}{\cosh(\mu D)}\,, \tag{30}$$

$$0=\left[1-\epsilon\mu D\tanh(\mu D\sigma)\eta\right]\eta_t-\frac{\tanh(\mu D\sigma)}{\mu D}\xi_{xx}^+-\epsilon(\eta\xi_x^+)_x\,, \tag{31}$$

where $D=(-\partial_{xx})^{1/2}$ with the Fourier symbol $|k|$. It follows directly that Eq. (29) can be used to decouple $\boldsymbol{\Phi}^b$ from the system. In the spirit of Whitham, who retained the full linear dispersion relation while deriving a weakly nonlinear model in the classical water-wave problem (Whitham, 1974), we keep the linear terms unchanged in the above three equations and apply the series expansion about $\mu=0$ in all the nonlinear terms. Thus, taking the Taylor expansions of the ϵ-related terms in Eqs. (30) and (31) around $\mu=0$ and retaining terms valid up to $\mathcal{O}\left(\epsilon,\mu^2\right)$, one obtains

$$\eta_t=\left[\frac{D\tanh(\mu D)}{\mu}-\epsilon\partial_x(\eta-b)\partial_x\right]\xi^-=-\left[\frac{D\tanh(\mu D\sigma)}{\mu}+\epsilon\partial_x\eta\partial_x\right]\xi^+\,, \tag{32}$$

where $\boldsymbol{\Phi}^b$ has been replaced with ξ^- due to (29). Eq. (32) gives the Taylor expansions of DNOs valid up to $\mathcal{O}\left(\epsilon,\mu^2\right)$, namely

$$G^-\approx\frac{D\tanh(\mu D)}{\mu}-\epsilon\partial_x(\eta-b)\partial_x\,,\qquad G^+\approx\frac{D\tanh(\mu D\sigma)}{\mu}+\epsilon\partial_x\eta\partial_x\,. \tag{33}$$

2.4. Whitham type equation

The dimensionless Hamiltonian reads

$$\mathcal{H}[\eta,\xi]=\frac{1}{2}\int_{\mathbb{R}}\left[\xi G^-\left(G^++RG^-\right)^{-1}G^+\xi+\eta^2\right]\mathrm{d}x\,, \tag{34}$$

where we denote by $R=\rho^+/\rho^-<1$ the density ratio between two fluids. Formally expanding the pseudo-differential operator $G^-\left(G^++RG^-\right)^{-1}G^+$ is crucial to derive a fully dispersive and weakly nonlinear model. Following (Whitham, 1974), we again keep the leading-order term, and take the Taylor expansion around $\mu=0$ for terms with η and b. By virtue of (33), we obtain, after a straightforward calculation,

$$G^-\left(G^++RG^-\right)^{-1}G^+=\frac{D\tanh(\mu D)\tanh(\mu D\sigma)}{\mu\left[\tanh(\mu D\sigma)+R\tanh(\mu D)\right]}+\frac{\epsilon(R-\sigma^2)}{(\sigma+R)^2}\partial_x\eta\partial_x$$
$$+\frac{\epsilon\sigma^2}{(\sigma+R)^2}\partial_xb\partial_x+\text{h.o.t.} \tag{35}$$

Substituting (35) into (34) and neglecting the higher-order terms, we obtain an approximate Hamiltonian as

$$\mathcal{H}[\eta,\xi]\approx\frac{1}{2}\int\left[\frac{\xi D\tanh(\mu D)\tanh(\mu D\sigma)\xi}{\mu\left[\tanh(\mu D\sigma)+R\tanh(\mu D)\right]}+\frac{\epsilon(\sigma^2-R)}{(\sigma+R)^2}\eta\xi_x^2\right.$$
$$\left.-\frac{\epsilon\sigma^2}{(\sigma+R)^2}b\xi_x^2+\eta^2\right]\mathrm{d}x\,. \tag{36}$$

And then, taking variational derivatives yields the model equations

$$\eta_t=\frac{\delta\mathcal{H}}{\delta\xi}=\mathcal{K}*\xi-\frac{\epsilon(\sigma^2-R)}{(\sigma+R)^2}(\eta\xi_x)_x+\frac{\epsilon\sigma^2}{(\sigma+R)^2}(b\xi_x)_x\,, \tag{37}$$

$$\xi_t=-\frac{\delta\mathcal{H}}{\delta\xi}=-\eta-\frac{\epsilon(\sigma^2-R)}{2(\sigma+R)^2}\xi_x^2\,. \tag{38}$$

Here the asterisk stands for convolution, and $\mathcal{K}$ is a pseudo-differential operator with the Fourier symbol

$$\widehat{\mathcal{K}}=\frac{|k|\tanh(\mu|k|)\tanh(\mu|k|\sigma)}{\mu\left[\tanh(\mu|k|\sigma)+R\tanh(\mu|k|)\right]}\,, \tag{39}$$

where the hat represents the Fourier transform. Eqs. (37)–(38) form a closed system for η and ξ, and the numerics for the system is not difficult to implement based on the fast Fourier transform technique (Aceves-Sánchez et al., 2013; Carter, 2018; Milewski and Tabak, 1999). Nonetheless, we can further convert these two first-order equations into a single second-order equation describing bidirectional propagations. Taking the time derivative of Eq. (38) and replacing η_t with Eq. (37), one obtains

$$\xi_{tt}+\mathcal{K}*\xi-\frac{\epsilon(\sigma^2-R)}{(\sigma+R)^2}(\eta\xi_x)_x+\frac{\epsilon\sigma^2}{(\sigma+R)^2}(b\xi_x)_x+\frac{\epsilon(\sigma^2-R)}{2(\sigma+R)^2}\left(\xi_x^2\right)_t=0\,. \tag{40}$$

Finally, replacing η with $-\xi_t$ gives

$$\xi_{tt}+\mathcal{K}*\xi+\frac{\epsilon(\sigma^2-R)}{(\sigma+R)^2}\left[\left(\xi_x^2\right)_t+\xi_t\xi_{xx}\right]+\frac{\epsilon\sigma^2}{(\sigma+R)^2}(b\xi_x)_x=0\,, \tag{41}$$

which is a generalization of the one-spatial-dimensional Benney–Luke equation (Yuan et al., 2020), termed the Whitham equation for internal waves. Returning to the dimensional variables, Eq. (41) becomes

$$\xi_{tt}+\mathcal{R}*\xi+\gamma\left[\left(\xi_x^2\right)_t+\xi_t\xi_{xx}\right]+\beta(b\xi_x)_x=0\,, \tag{42}$$

where

$$\widehat{\mathcal{R}}=\frac{g(1-R)|k|\tanh(h^-|k|)\tanh(h^+|k|)}{\tanh(h^+|k|)+R\tanh(h^-|k|)}\,,\quad \gamma=\frac{\sigma^2-R}{(\sigma+R)^2}\,,$$
$$\beta=\frac{g(1-R)\sigma^2}{(\sigma+R)^2}\,. \tag{43}$$

Finally, the fluctuation of the interface $\eta(x,t)$ can be rewritten in the dimensional variables as, to the leading order approximation of Eq. (38),

$$\eta = -\frac{\xi_t}{g(1-R)}\,. \tag{44}$$

While the Whitham Eq. (42) is a bidirectional propagation model, its simplified version, the unidirectional equation, is sometimes adequate to delineate practical scenarios. Indeed, the Whitham equation was initially proposed as a unidirectional model to describe breaking and peaking in shallow water, the phenomena contained in the full Euler equations but not in the KdV theory. Following Whitham's idea, assuming one-way propagation and combining full linear dispersion with long wave nonlinearity, the unidirectional Whitham type model for interfacial waves can be expressed as

$$\eta_t + \mathscr{H}\left[\Re^{\frac{1}{2}} * \eta\right] + \alpha\eta\eta_x = 0\,, \tag{45}$$

where $\mathscr{H}$ represents the Hilbert transform and acts on the Fourier symbol to render $\mathrm{i}\,\mathrm{sgn}(k)$, and the quadratic nonlinear coefficient α is

$$\alpha = \frac{3}{2}\sqrt{\frac{g(1-R)}{(\sigma+R)h^+}}\left(\frac{\sigma^2-R}{\sigma+R}\right). \tag{46}$$

Nevertheless, one of the most widely-used models for internal waves, the KdV type equation (Grimshaw et al., 2002), can be derived directly from the Whitham-type equations by expanding and truncating the pseudo-differential operator. Thus, the KdV equation is generally written as

$$\eta_t + c_0\eta_x + \alpha\eta\eta_x + \lambda\eta_{xxx} = 0\,. \tag{47}$$

Here the nonlinear coefficient α is the same as Eq. (46), whereas the linear phase speed c_0 and dispersive coefficient λ are given by

$$c_0^2 = \frac{g(1-R)h^+}{\sigma+R}\,, \quad \lambda = \frac{(Rh^+ + h^-)h^+\sqrt{g(1-R)h^+}}{6(\sigma+R)^{3/2}}\,. \tag{48}$$

More importantly, it is well-known that the KdV Eq. (47) admits of a soliton solution, analytically represented as

$$\eta = \eta_0\,\mathrm{sech}^2\left[\sqrt{\frac{\alpha\eta_0}{12\lambda}}\,x - \left(c_0 + \frac{\eta_0\alpha}{3}\right)t\right], \tag{49}$$

where η_0 is the wave amplitude. The linear dispersion relations of the KdV Eq. (47) and the Whitham type Eqs. (42), (45) are

$$\omega = c_0 k - \lambda k^3 \quad \text{and} \quad \omega^2 = \frac{g(1-R)|k|\tanh(h^-|k|)\tanh(h^+|k|)}{\tanh(h^+|k|) + R\tanh(h^-|k|)}\,, \tag{50}$$

respectively. These results are illustrated in non-dimensional forms in Fig. 2. We immediately note an important consequence that the linear speeds (either the phase speed $c = \omega/k$ or the group speed $c_g = \mathrm{d}\omega/\mathrm{d}k$) of these two equations are very close when long waves are considered with $k \approx 0$, which, however, become diverse as the evolution being away from the regime of the longwave. More significantly, the phase velocity of the KdV equation becomes negative for sufficient short waves (large wavenumber k), contradicting the original assumption of forward-propagation waves. In contrast, our proposed Whitham type equations retain the full linear dispersion relation of the Euler equations, and as a result, $c \to 0$ and $c_g \to 0$ as $k \to \infty$. These results imply some potential advantage of our proposed Whitham type equations for some cases of practical interest.

3. Numerical results

3.1. Numerical method

Note that it is challenging to obtain general solutions to the Whitham type equations, and thus we have to resort to a numerical method. Considering the second term of the Whitham Eq. (42) involving a pseudo-differential operator, we, naturally, propose a numerical scheme based on the fast Fourier transform implemented with a pseudo-spectral method, refer to Milewski and Tabak (1999). The Whitham Eq. (42) can be rewritten as

$$\left(\frac{\partial^2}{\partial t^2} + \mathcal{L}^2\right)\xi = \mathcal{N}(b,\xi,\xi_t,)\,, \tag{51}$$

where the operator $\mathcal{L} = \Re^{\frac{1}{2}}$, and $\mathcal{N}$ represents both the nonlinear and topographic terms. Since our derived Whitham equation retains the full dispersion of the Euler equations, the operator $\mathcal{L}$ gives rise to a wide range of time scales, while the comparatively slow evolution influenced by nonlinearity $\mathcal{N}$ is often of research interest. However, to study this slow evolution, the fast frequencies associated with $\mathcal{L}$ have to be resolved, which practically renders the selection of tiny time steps in numerical simulations. To circumvent the stiffness problem, we introduce one intermediate variable,

$$\varphi = \left(\frac{\partial}{\partial t} + \mathrm{i}\,\mathcal{L}\right)\xi\,, \tag{52}$$

and as a result, Eq. (51) reduces to a temporally first-order equation

$$\left(\frac{\partial}{\partial t} - \mathrm{i}\,\mathcal{L}\right)\varphi = \mathcal{N}(b,\xi,\xi_t)\,. \tag{53}$$

Note that ξ and ξ_t can be calculated from the real part and imaginary parts of φ:

$$\xi_t = \mathrm{Re}\,(\varphi)\,, \quad \mathcal{L}\xi = \mathrm{Im}\,(\varphi)\,, \tag{54}$$

which implies that Eq. (53) is a single evolution equation with one unknown φ. Next, applying the Fourier transform to this equation in x yields

$$\left(\frac{\partial}{\partial t} - \mathrm{i}\,\widehat{\mathcal{L}}\right)\widehat{\varphi}(k,t) = \mathcal{F}\left[\mathcal{N}(b,\xi,\xi_t)\right](k,t)\,, \tag{55}$$

where both $\widehat{\cdot}$ and $\mathcal{F}$ represent the Fourier transform. Then, multiplying the above equation by an integrating factor, $e^{-\mathrm{i}\widehat{\mathcal{L}}t}$, yields

$$\frac{d\widehat{\vartheta}}{dt} = e^{-\mathrm{i}\,\widehat{\mathcal{L}}t}\mathcal{F}\left[\mathcal{N}(b,\xi,\xi_t)\right], \quad \text{where } \widehat{\vartheta} = e^{-\mathrm{i}\,\widehat{\mathcal{L}}t}\widehat{\varphi}\,. \tag{56}$$

The variations of fast frequencies, which, if not appropriately resolved with a small time step, yield numerical instabilities in Eqs. (51) and (53), have been rearranged at the right-hand side of (56). It was shown that this rearrangement overcomes the difficulty of stiffness, and hence a larger time step can be chosen. In practice, what remains is to relate $\widehat{\vartheta}$ or $\widehat{\varphi}$ with ξ and ξ_t. It can be achieved by manipulating the Fourier transform of Eq. (52), which ultimately gives:

$$\xi_t = \mathcal{F}^{-1}\left\{\frac{\widehat{\varphi}(k,t) + \widehat{\varphi}^*(-k,t)}{2}\right\}, \quad \xi = \mathcal{F}^{-1}\left\{\frac{\widehat{\varphi}(k,t) - \widehat{\varphi}^*(-k,t)}{\mathrm{i}\left[\widehat{\mathcal{L}}(k) + \widehat{\mathcal{L}}(-k)\right]}\right\}, \tag{57}$$

where the superscript asterisk designates complex conjugation and $\mathcal{F}^{-1}$ stands for the inverse Fourier transform. Nevertheless, one difficulty is that ξ cannot be recovered from Eq. (57) for $k = 0$, as the denominator equals zero, $\widehat{\mathcal{L}}(0) = 0$, but instead, it can be numerically evaluated by integrating the ξ_t equation. In the temporal domain, we choose the classic 4th-order Runge–Kutta scheme with typical time step of 0.2 s.

3.2. Wave evolution

To examine the abilities of these equations on delineating the wave evolution, in the following sections, we design several numerical experiments. In all cases, the thicknesses are $h^+ = 100\,\mathrm{m}$ and $h^- = 300\,\mathrm{m}$ from top to bottom, while the respective densities are $\rho^+ = 1000.8\,\mathrm{kg/m^3}$ and $\rho^- = 1012.0\,\mathrm{kg/m^3}$, which corresponds to 5 PSU and 20 PSU at temperature 25°C in the ocean, refer to Millero and Poisson (1981). First, we choose a 'box' as the initial condition to launch the simulation, whereby internal undular bores (also called dispersive shock waves) and linear ramps with trailing oscillations are rendered. It is noted that undular bores are rank-ordered waves whose nonlinearities decrease

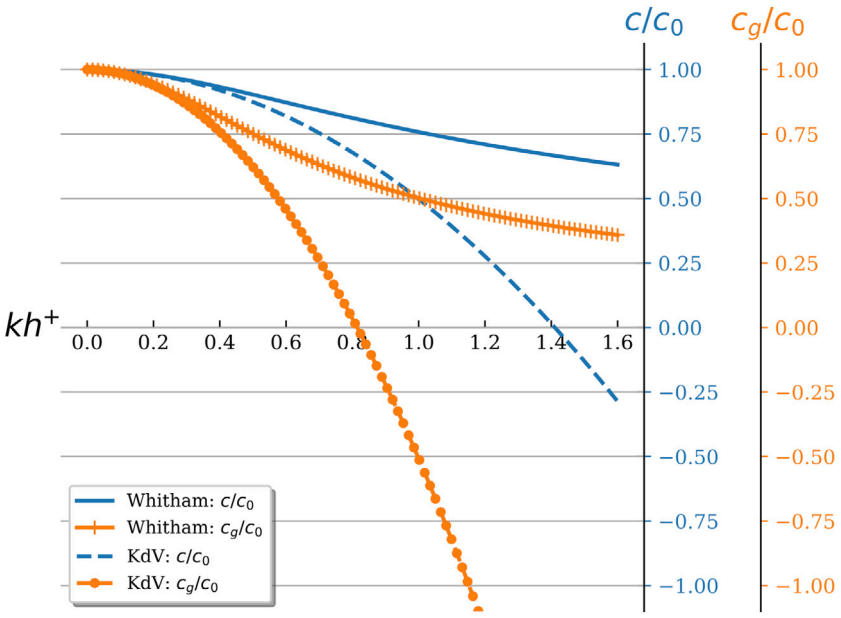

Fig. 2. Dimensionless linear dispersion relations of the KdV equation and the Whitham equation. Note that the wavenumber k is normalized by the thickness of upper layer h^+, while both the linear phase speed c and group speed c_g are normalized by c_0 as given in Eq. (48).

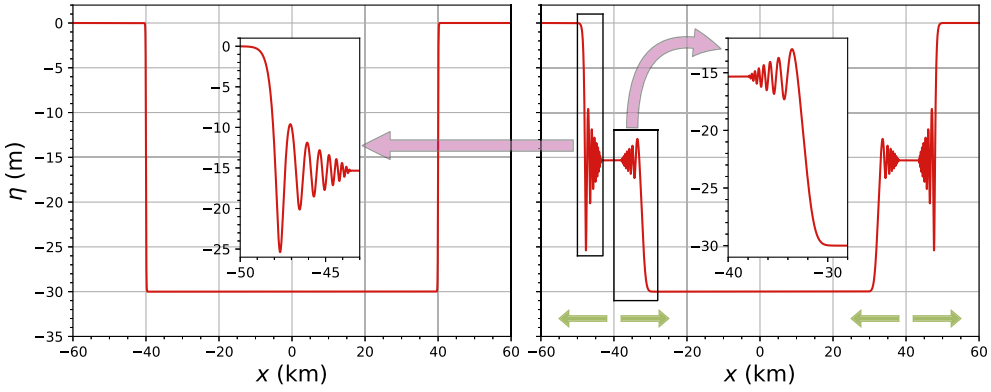

Fig. 3. Left panel: initial box as given in Eq. (58) with the amplitude $A_0 = -30$ m and width $2\varkappa = 80$ km. Right panel: evolution results of the initial box with zero horizontal particle velocity launched at $t = 2700$ s. Note that the resultant internal undular bores and linear ramps with trailing oscillations, along with their propagation directions, are accentuated using insets and green arrows. (For interpretation of the references to color in this figure legend, the reader is referred to the web version of this article.)

from the solitary waves in the front to the periodic waves in the rear, see Fig. 3 as an example.

Considering the length of the domain in the x-direction is about 100 km (resolved by $2^{15} = 32768$ discrete points), the initial box is expressed as

$$\eta(x, t = 0) = \frac{1}{2} A_0 \left\{ \tanh\left[\frac{x + \varkappa}{500}\right] - \tanh\left[\frac{x - \varkappa}{500}\right] \right\}, \tag{58}$$

where $A_0 = -9$ m and $\varkappa = 4$ km in the unidirectional Whitham equation and the KdV equation, see Fig. 4. The choice of the minus sign is attributed to the fact that the thicknesses of two layers, $h^- > h^+$, support the survival of depression leading waves, which designates negative amplitude in our coordinate system. To conduct a quantitative comparison, we choose $A_0 = -18$ m in the bidirectional Whitham equation, as here the initial box will evolve towards two symmetric wave patterns, each possessing the height half of its startup and propagating along with opposite directions. Another issue is that the bidirectional Whitham equation needs both ξ and ξ_t to be given as the initial conditions, where $\xi_t(t = 0)$ can be easily calculated from $\eta(t = 0)$ according to Eq. (44). It remains to determine $\xi(t = 0)$; here we use $\xi(t = 0) = 0$ and hence $\xi_x(t = 0) = 0$, which means that the initial horizontal particle velocity is set to be zero.

The results are illustrated in Fig. 4, in which the results of the unidirectional and bidirectional Whitham equations do not exhibit perceptible disparities. By contrast, differences between the KdV equation and the Whitham type equations are clearly shown in the figure, where the latter equations feature larger amplitude and faster speed, a phenomenon similar to the comparison between the KdV and Whitham equations in surface water waves (Carter, 2018). Note that the unidirectional Whitham equation and the KdV equation have the same nonlinearity but the latter with less accurate dispersion, given the fact that the Whitham type equations reproduce the Euler phase and group speeds; see Fig. 2. To validate these reduced theoretical models, We conduct simulations based on a fully nonlinear non-hydrostatic MIT general circulation model (MITgcm) (Marshall et al., 1997). Although the MITgcm model numerically solves the incompressible Navier–Stokes equations with the Boussinesq assumption, it amounts to solving the stratified Euler equations by setting the viscosity coefficients in the momentum equations and diffusion coefficient in the salinity equation to be zero (here, the temperature is treated as a constant). The setups in the MITgcm model are the same as those in the theoretical models. Free boundary conditions suffice to simulate this localized phenomenon considering the given large domain (~ 200 km) in Fig. 4.

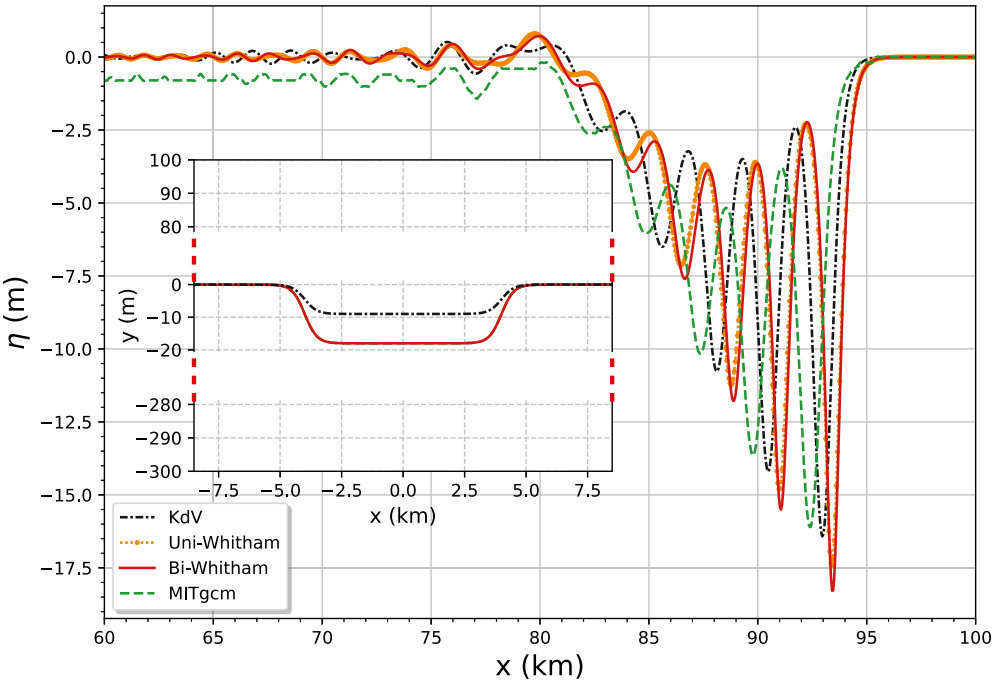

Fig. 4. Evolutions of the initial boxes (shown in the inset) in the KdV, unidirectional Whitham (labeled as Uni-Whitham), bidirectional Whitham (labeled as Bi-Whitham) equations, and the MITgcm model at $t = 3.0 \times 10^4$ s. Note that the height of the initial boxes for the KdV and Uni-Whitham equations is half of that for the Bi-Whitham equation and the MITgcm model.

It is clear that the wave amplitudes in the MITgcm model are smaller than those in the theoretical models, and the reason can be partly ascribed to the numerical truncation errors and numerical viscosity. In addition, a continuous stratification is generally needed for the MITgcm model. Hence the used two-layer configurations must be subject to a redistribution of salinity (as the temperature is settled as uniform, so the salinity is treated as a passive tracer). It then leads to a thin pycnocline whose dynamical manner will be essentially distinguished from the standard two-layer set-ups. Nevertheless, the wave patterns are genuinely similar, suggesting the validity of these reduced theoretical models.

To further confirm the accuracy of our proposed models, we design numerical experiments with Gaussian initial conditions,

$$\eta(x, t = 0) = A_0 \exp\left[-\left(\frac{x}{5000}\right)^2\right], \tag{59}$$

where the initial amplitudes $A_0 = -10$ m for the unidirectional Whitham equation and the KdV equation, but $A_0 = -20$ m for the bidirectional Whitham equation, see Fig. 5. The initial lumps evolve to get trains of rank-ordered solitary waves in all models. Although the KdV equation manifests itself with smaller amplitude and slower speed, the number of the emerged solitons is the same, and the wave pattern is also similar.

Although Ehrnström et al. (2012) proved that solitary-wave solutions exist in the Whitham type equations, it is challenging to obtain the explicit expressions. Thus, we suggest a numerical method based on the Petviashvili iteration to find the solutions. The basic idea is to perform the iteration in the Fourier space supplemented by a normalization factor upon the degree of nonlinearity. Assuming a wave propagates in the x-direction with a translating speed c, then applying the Fourier transform to Eq. (42) leads to

$$\widehat{\xi} = \frac{c\gamma\left(\mathrm{i}k\widehat{\xi_x^2} + \widehat{\xi_x \xi_{xx}}\right)}{\widehat{\mathfrak{K}} - c^2k^2} \triangleq \mathcal{Q}[\widehat{\xi}]. \tag{60}$$

Following Ablowitz et al. (2006), a multiplier is introduced in every iteration step to prevent amplitude from going into zero or infinity, that is

$$\widehat{\xi}_{n+1} = \tau_n \mathcal{Q}[\widehat{\xi}_n], \tag{61}$$

where the subscript n indicates the index of iteration step and τ_n is given by

$$\tau_n = \frac{\int |\widehat{\xi}_n|^2 dk}{\int \widehat{\xi}_n^* \mathcal{Q}[\widehat{\xi}_n] dk}. \tag{62}$$

In practice, to obtain the solutions describing internal solitary waves in the Whitham type equations, the KdV solitary wave solution (49) can be used to launch this iteration. The iteration process will be terminated when the relative error χ,

$$\chi = \frac{\sum_m |\widehat{\xi}_{n+1} - \widehat{\xi}_n|}{\sum_m |\widehat{\xi}_n|}, \tag{63}$$

is smaller than some specific value (we select 1.0×10^{-17} in the related experiments hereafter), where m represents the index of discrete points.

Using the solitary-wave solutions obtained with the aforementioned Petviashvili iteration method to prepare the initial condition, we investigate the overtaking collision between a large internal solitary wave with an amplitude of 20 m and a small wave with an amplitude of 4 m in Fig. 6. When the large wave approaches the small one, the discrepancies between the bidirectional and unidirectional models emerge. The large-amplitude solitary wave in the bidirectional Whitham equation features a relatively slower speed and a slightly smaller amplitude than in the unidirectional model, see panel (b). These discrepancies evolve to become more and more sensible afterward, as shown in panels (c) and (d). The evolution behaviors of the small-amplitude solitary waves in the bi- and uni-directional Whitham equations are almost the same, differing from that in the KdV equation. Although there are no perceptible disparities between the two unidirectional models before collision (panels (a) and (b)), separation commences after the large wave surpasses the small one (panel (c)). Nonetheless, it showcases that the overtaking collision leads to phase lags of the small wave and phase advances of the large wave in all three models, albeit to a different extent, see panel (d). Noticeably, these discrepancies and similarities may be a result of the combination of linear and nonlinear effects, both of which can modify the wave propagation velocity.

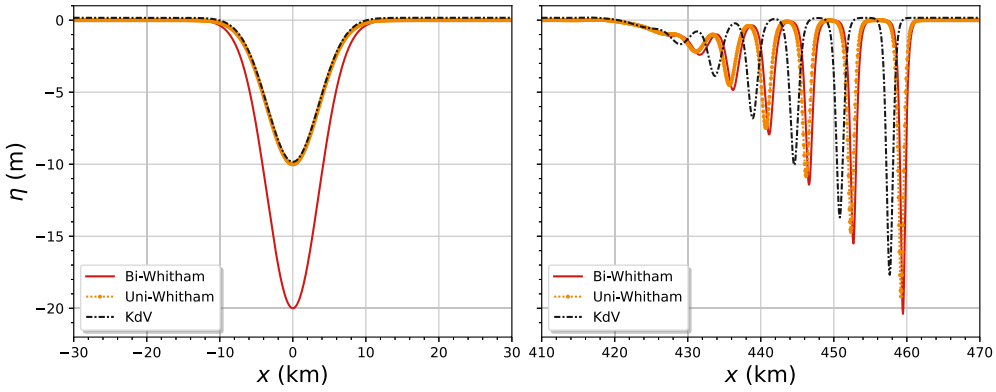

Fig. 5. Left panel: Gaussian initial conditions. Right panel: snapshots of wave profile at $t = 1.5 \times 10^5$ s.

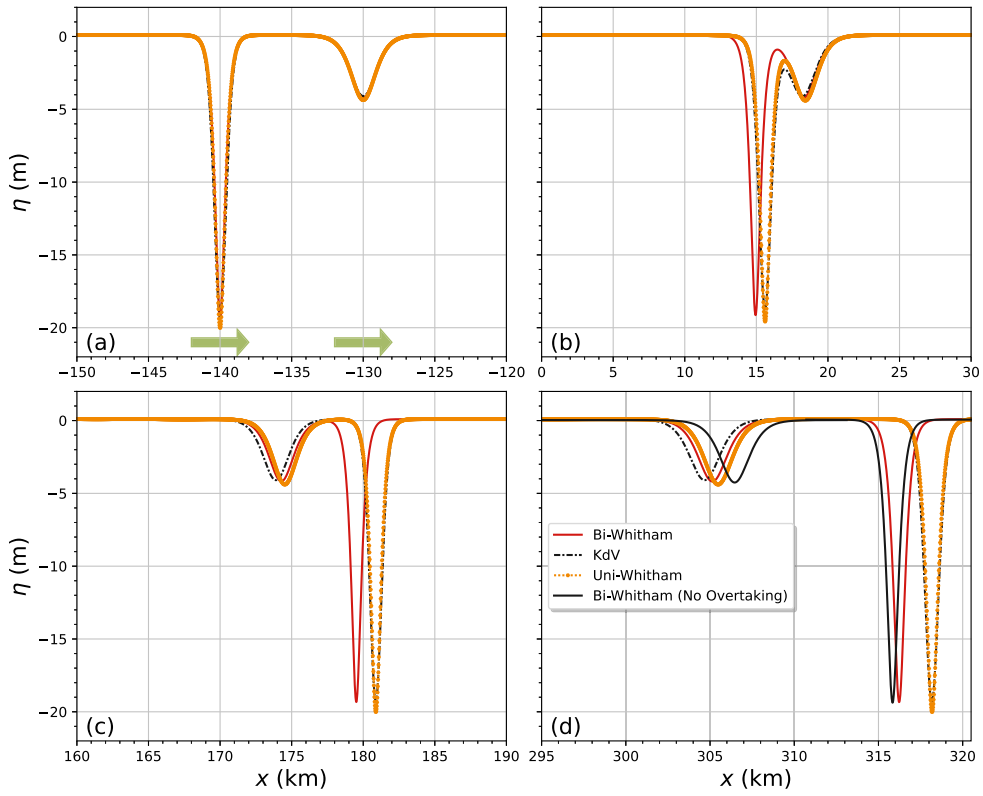

Fig. 6. Overtaking collision between a large-amplitude internal solitary wave ($\max|\eta| = 20$ m) and a small-amplitude one ($\max|\eta| = 4$ m): (a) $t = 0$ s, (b) $t = 5.1 \times 10^4$ s, (c) $t = 1.05 \times 10^5$ s, (d) $t = 1.5 \times 10^5$ s. For comparison, evolutions of the respective waves without collision are plotted as the dark solid line at $t = 1.5 \times 10^5$ s in panel (d).

Among the above-mentioned reduced models, the bidirectional Whitham type equation is the only one suitable for simulating nonlinear interactions between two oppositely propagating waves. Here we examine the head-on collision between an internal solitary wave and an internal undualr bore in Fig. 7. With passing through the undular bore, the persistent waveform of the solitary wave begins to destruct, owing to the nonlinear interactions between these two waves. The leading wave features a smaller amplitude and a slower speed, with a trailing oscillation emerging in the rear. Meanwhile, the undular bore undergoes a slight phase shift, although no perceptible waveform changing is found (see panel (d)). As shown in Fig. 3, a box with zero initial horizontal velocity will render, in addition to undular bores, linear ramps with trailing oscillations. Indeed, Ablowitz et al. (2018) investigated a solitary wave collide with a linear ramp in the KdV dynamics. These authors solved the problem by using the inverse scattering transform method and showed that the interaction dynamics depend on the amplitude of the solitary wave. If the amplitude is large enough, a proper spectral data solution indicates that the solitary wave can pass through the linear ramp; however, if the amplitude is under a threshold, the solitary wave will be trapped inside the rarefaction ramp. Here we try to reproduce these interesting phenomena in the Whitham equation, and the results are illustrated in Fig. 8. Except for the expected scenarios of tunneling and trapped solitary waves, we also find that, after the collision, the amplitudes of solitary waves become smaller in both cases, which will naturally result in lower propagation speeds.

One of the significant modifications we made on the Whitham type equation is that, in the derivation, the bottom topographic effects are considered. Since the scalings (22) assumed that the height of topography is the same order as that of the interface amplitude, thus significant topography is presumably inappropriate, and here we would not risk doing this. However, the validity range needs more research to be determined. In Fig. 9, referring to the typical cases in the real ocean, we put a gentle shoaling topography below an initial solitary

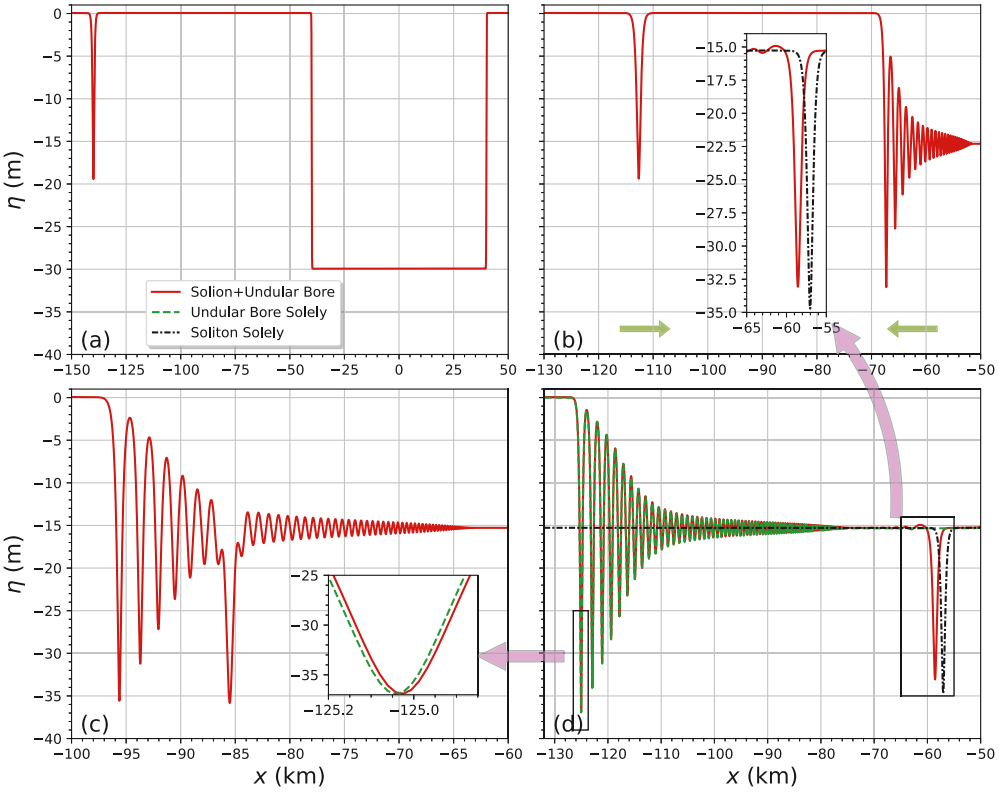

Fig. 7. Collision between an internal solitary wave and an undular bore. Note that an initial box is used to generate the undular bore as shown in panel (a). Panels (b–d): snapshots of wave profile at $t = 9.0 \times 10^3$ s, $t = 1.8 \times 10^4$ s, and $t = 2.7 \times 10^4$ s. Two zoom-ins are inserted to accentuate the waveform. For comparison, the evolution results of a single solitary wave and an undular bore without collision are exhibited in dark densely dashed lines and green loosely dashed lines, respectively.

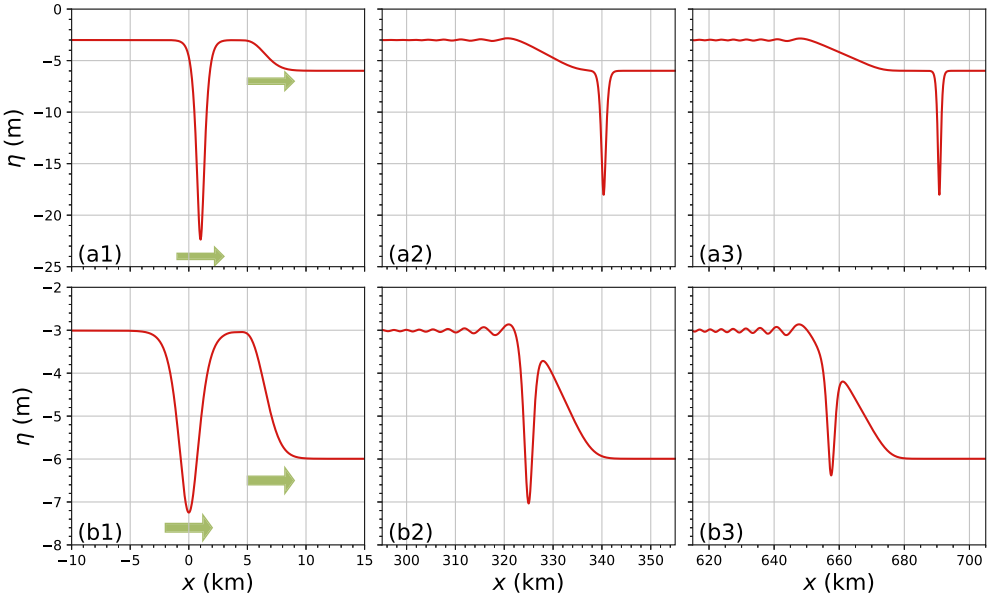

Fig. 8. Interactions between internal solitary waves and linear ramps. Panels (a1–a3): snapshots of tunneling solitary wave at $t = 0$ s, $t = 1.13 \times 10^5$ s, and $t = 2.3 \times 10^5$ s. Panels (b1–b3): snapshots of trapped solitary wave at $t = 0$ s, $t = 1.13 \times 10^5$ s, and $t = 2.3 \times 10^5$ s. Note that the propagation directions are illustrated in green arrows.

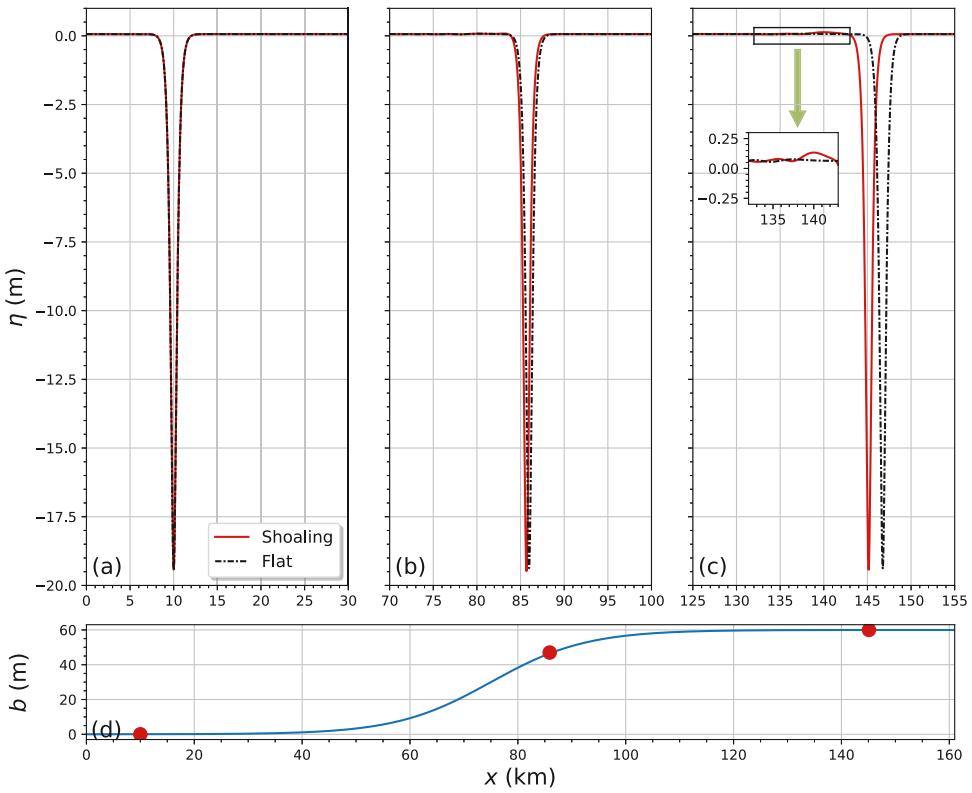

Fig. 9. Evolution of a solitary wave propagating over a mild topography. Wave profiles at $t = 0$ s, $t = 2.5 \times 10^4$ s, and $t = 4.5 \times 10^4$ s are shown in panels (a–c). The shoaling topography considered is plotted in panel (d), where read dots indicate locations of the solitary wave in panels (a–c). Note that, for comparison, the wave evolution without topography is also illustrated by the dark dashed line.

wave to check the effectiveness of the Whitham equation. It is clear that the shoaling topography slackens the wave propagation and augments the wave amplitude; more importantly, some small trailing wavetrains appear in the rear of the leading solitary waves.

4. Conclusion

The pioneering works on the Whitham type equations are Whitham and Lighthill (1967) and Whitham (1974) for free-surface waves, and they have attracted researchers' attention in the last several decades. Of note is the work of Aceves-Sánchez et al. (2013) and Moldabayev et al. (2015) who extended Whitham's idea to study bidirectionally propagating surface waves, Aceves-Sánchez et al. (2013) and Vargas-Magaña and Panayotaros (2016) who examined the varying topographic effects on wave dynamics using the modified Whitham type equations, Dinvay et al. (2017) and Carter (2018) who took the surface tension into account, and Dinvay et al. (2019) and Wang (2022) who generalized the equation to describe hydroelastic waves. In addition to these, the properties of the Whitham equations have been explored by Ehrnström and Kalisch (2009, 2013), Sanford et al. (2014) and Hur and Johnson (2015) amongst many others. Aceves-Sánchez et al. (2013) claimed that peaked soliton solutions are accommodated in the Whitham type equations, in addition to smooth solitary-wave solutions (Ehrnström et al., 2012). More importantly, Carter (2018) conducted a series of comparisons between laboratory experiments and seven theoretical reduced models (including the KdV equation) to show that the Whitham type equations provide more accurate approximations than others. This accuracy was also confirmed in Moldabayev et al. (2015).

The advantage of the Whitham type equations and the previous research on this subject inspire us to derive the same type of equation for internal waves. We have utilized the Hamiltonian formulation of the two-layer fluid system and expanded the kinetic energy associated with the Dirichlet–Neumann operators to derive a Whitham type equation. The newly developed equation is a fully dispersive and weakly nonlinear model with bidirectional propagations. To make it more suitable for practice interest, we have involved a term representing the effects of varying topography in the model equation. This model can also yield a unidirectional Whitham type equation by assuming a one-way propagation.

The KdV equation is the most widely-used theoretical reduced model for investigating wave dynamics and interpreting *in-situ* observational data. However, the characters of unidirectional-propagation assumption and unbounded phase and group velocities imply an inappropriate model for some general cases (say, for example, head-on collisions between solitary waves), see Benjamin et al. (1972) for more details. The proposed Whitham type equations overcome these shortcomings, and the comparisons with the KdV equation and the MITgcm model confirm this point. The disparities between the KdV equation and the Whitham type equations provide new insight into wave dynamics and embody the importance of full dispersion and bidirectional propagation. We have also investigated the solitary wave colliding with undular bore, which is not suitable to be examined with unidirectional models.

Finally, it is necessary to indicate the shortcomings of the Whitham type equations. Although the proposed equation plausibly possesses a concise form, finding its analytical solitary-wave solutions is challenging. In this paper, we suggest a modified Petviashvili iteration method to numerically search for solitary waves, which, however, highly depends on the given initial guess, as the equation may admit of more than one type of solution, say the cusped soliton and the form close to the sech-squared function (Aceves-Sánchez et al., 2013). Note that the effects of variable topography are taken into account, but we caution that much care should be given when significant topography is involved. Except that, the stratification is approximated to a two-layer scheme, and it is a good approximation for some cases. Nonetheless, sometimes, we still need to consider the continuous stratification. Yuan

and Wang (2022) showed a layering scheme to determine the respective thickness and density of each layer based on the continuous stratification. This method can maintain the kinematical equivalence to the most considerable extent and undoubtedly be combined with the Whitham type equations.

CRediT authorship contribution statement

Chunxin Yuan: Software, Visualization, Writing. **Zhan Wang:** Conceptualization, Methodology, Writing.

Declaration of competing interest

The authors declare that they have no known competing financial interests or personal relationships that could have appeared to influence the work reported in this paper.

Acknowledgments

This work was supported by the National Natural Science Foundation of China (Nos. 11911530171, 11772341, 42006016), the key program of the National Natural Science Foundation of China (Nos. 12132018, 91958206), and the Natural Science Foundation of Shandong Province, China (No. ZR2020QD063).

References

Ablowitz, M.J., Fokas, A.S., Musslimani, Z.H., 2006. On a new non-local formulation of water waves. J. Fluid Mech. 562, 313–343.

Ablowitz, M.J., Luo, X.-D., Cole, J.T., 2018. Solitons, the Korteweg-de Vries equation with step boundary values, and pseudo-embedded eigenvalues. J. Math. Phys. 59, 091406.

Aceves-Sánchez, P., Minzoni, A., Panayotaros, P., 2013. Numerical study of a nonlocal model for water-waves with variable depth. Wave Motion 50, 80–93.

Andrade, D., Nachbin, A., 2018. A three-dimensional Dirichlet-to-Neumann operator for water waves over topography. J. Fluid Mech. 845, 321–345.

Barker, A., 2021. Indonesia's sunken submarine may have been hit by a powerful force known as an internal wave. URL https://www.abc.net.au/news/2021-04-30/indonesian-submarine-may-have-been-hit-by-internal-wave/100102816.

Barros, R., Choi, W., Milewski, P.A., 2020. Strongly nonlinear effects on internal solitary waves in three-layer flows. J. Fluid Mech. 883, A16.

Benjamin, T.B., 1966. Internal waves of finite amplitude and permanent form. J. Fluid Mech. 25 (2), 241–270.

Benjamin, T.B., Bona, J.L., Mahony, J.J., 1972. Model equations for long waves in nonlinear dispersive systems. Philos. Trans. R. Soc. Lond. Ser. A 272, 47–78.

Benjamin, T.B., Bridges, T.J., 1997. Reappraisal of the Kelvin–Helmholtz problem. Part 1. Hamiltonian structure. J. Fluid Mech. 333, 301–325.

Cai, S., Gan, Z., 2001. Progress in the study of the internal solition in the Northern South China sea (in Chinese). Adv. Earth Sci. 16 (2), 215–219.

Cai, S., Xie, J., 2010. A propagation model for the internal solitary waves in the northern South China sea. J. Geophys. Res. Oceans 115 (C12074).

Carter, J.D., 2018. Bidirectional Whitham equations as models of waves on shallow water. Wave Motion 82, 51–61.

Choi, W., Camassa, R., 1999. Fully nonlinear internal waves in a two-fluid system. J. Fluid Mech. 396, 1–36.

Craig, W., Guyenne, P., Nicholls, D.P., Sulem, C., 2005. Hamiltonian long-wave expansions for water waves over a rough bottom. Proc. R. Soc. Lond. Ser. A Math. Phys. Eng. Sci. 461, 839–873.

Craig, W., Guyenne, P., Sulem, C., 2012. The surface signature of internal waves. J. Fluid Mech. 710, 277–303.

Craig, W., Sulem, C., 1993. Numerical simulation of gravity waves. J. Comput. Phys. 108 (1), 73–83.

Dinvay, E., Kalisch, H., Moldabayev, D., Părău, E.I., 2019. The Whitham equation for hydroelastic waves. Appl. Ocean Res. 89, 202–210.

Dinvay, E., Moldabayev, D., Dutykh, D., Kalisch, H., 2017. The Whitham equation with surface tension. Nonlinear Dynam. 88, 1125–1138.

Djordjevic, V.D., Redekopp, L.G., 1978. The fission and disintegration of internal solitary waves moving over two-dimensional topography. J. Phys. Oceanogr. 8 (6), 1016–1024.

Duchene, V., 2014. On the rigid-lid approximation for two shallow layers of immiscible fluids with small density contrast. J. Nonlinear Sci. 24, 579–632.

Ehrnström, M., Groves, M.D., Wahlén, E., 2012. On the existence and stability of solitary-wave solutions to a class of evolution equations of Whitham type. Nonlinearity 25 (10), 2903–2936.

Ehrnström, M., Kalisch, H., 2009. Traveling waves for the Whitham equation. Differential Integral Equations 22, 1193–1210.

Ehrnström, M., Kalisch, H., 2013. Global bifurcation for the whitham equation. Math. Model. Nat. Phenom. 8, 13–30.

Fokas, A.S., Nachbin, A., 2012. Water waves over a variable bottom: a non-local formulation and conformal mappings. J. Fluid Mech. 695, 288–309.

Grimshaw, R., 1981. Evolution equations for long, nonlinear internal waves in stratified shear flows. Stud. Appl. Math. 65 (2), 159–188.

Grimshaw, R., Pelinovsky, E., Poloukhina, O., 2002. Higher-order Korteweg-de Vries models for internal solitary waves in a stratified shear flow with a free surface. Nonlinear Process. Geophys. 9, 221–235.

Grimshaw, R., Wang, C., Li, L., 2016. Modelling of polarity change in a nonlinear internal wave train in Laoshan Bay. J. Phys. Oceanogr. 46 (3), 965–974.

Guo, C., Chen, X., 2014. A review of internal solitary wave dynamics in the northern south China sea. Prog. Oceanogr. 121, 7–23.

Hur, V., Johnson, M., 2015. Modulational instability in the whitham equation for water waves. Stud. Appl. Math. 134, 120–143.

Jiang, S.W., Kovačič, G., Zhou, D., Cai, D., 2019. Modulation-resonance mechanism for surface waves in a two-layer fluid system. J. Fluid Mech. 875, 807–841.

Joseph, R., 1977. Solitary waves in a finite depth fluid. J. Phys. A 10 (12), L225–L227.

Kadomtsev, B.B., Petviashvili, V.I., 1970. On the stability of solitary waves in weakly dispersing media. Sov. Phys. Doklady 15, 539–541.

Klymak, J.M., Pinkel, R., Liu, C.-T., Liu, A.K., David, L., 2006. Prototypical solitons in the south China sea. Geophys. Res. Lett. 33 (11), L11607.

Kubota, T., Ko, D., Dobbs, L., 1978. Weakly-nonlinear, long internal gravity waves in stratified fluids of finite depth. J. Hydronaut. 12 (4), 157–165.

Li, L., Wang, C., Grimshaw, R., 2015. Observation of internal wave polarity conversion generated by a rising tide. Geophys. Res. Lett. 42 (10), 4007–4013.

Marshall, J., Adcroft, A., Hill, C., Perelman, L., Heisey, C., 1997. A finite-volume, incompressible Navier Stokes model for studies of the ocean on parallel computers. J. Geophys. Res. Oceans 102 (C3), 5753–5766.

Meyer, C.Y., 1985. Nonlinear harmonic analysis and analytic dependence. Proc. Sympos. Pure Math. 43, 71–78.

Milewski, P.A., Tabak, E.G., 1999. A PseudoSpectral procedure for the solution of nonlinear wave equations with examples from free-surface flows. SIAM J. Sci. Comput. 21 (3), 1102–1114.

Millero, F.J., Poisson, A., 1981. International one-atmosphere equation of state of seawater. Deep Sea Res. A 28 (6), 625–629.

Miyata, M., 1988. Long internal waves of large amplitude. In: Horikawa, K., Maruo, H. (Eds.), Nonlinear Water Waves. Springer Berlin Heidelberg, Berlin, Heidelberg, pp. 399–406.

Moldabayev, D., Kalisch, H., Dutykh, D., 2015. The Whitham equation as a model for surface water waves. Physica D 309, 99–107.

Ono, H., 1975. Algebraic solitary waves in stratified fluids. J. Phys. Soc. Japan 39 (4), 1082–1091.

Osborne, A.R., Burch, T.L., 1980. Internal solitons in the Andaman sea. Science 208 (4443), 451–460.

Ostrovsky, L.A., 1978. Nonlinear internal waves in a rotating ocean. Oceanology 18, 119–125.

Ostrovsky, L.A., Stepanyants, Y.A., 2005. Internal solitons in laboratory experiments: Comparison with theoretical models. Chaos 15 (3), 037111.

Ramp, S., Tang, T.Y., Duda, T., Lynch, J., Liu, A., Chiu, C.-S., Bahr, F., Kim, H.-R., Yang, Y.-J., 2004. Internal solitons in the northeastern south China sea. Part I: sources and deep water propagation. IEEE J. Ocean. Eng. 29 (4), 1157–1181.

Sanford, N., Kodama, K., Carter, J.D., Kalisch, H., 2014. Stability of traveling wave solutions to the Whitham equation. Phys. Lett. A 378, 2100–2107.

Shroyer, E.L., Moum, J.N., Nash, J.D., 2010. Mode 2 waves on the continental shelf: Ephemeral components of the nonlinear internal wavefield. J. Geophys. Res. Oceans 115 (C7), C07001.

Simmons, H., Chang, M.-H., Chang, Y.-T., Chao, S.-Y., Fringer, O., Jackson, C.R., Ko, D.S., 2011. Modeling and prediction of internal waves in the south China sea. Oceanography 24 (4), 88–99.

Tung, K.-K., Chan, T.F., Kubota, T., 1982. Large amplitude internal waves of permanent form. Stud. Appl. Math. 66 (1), 1–44.

Vargas-Magaña, R., Panayotaros, P., 2016. A Whitham–Boussinesq long-wave model for variable topography. Wave Motion 65, 156–174.

Wang, Z., 2022. A universal bifurcation mechanism arising from progressive hydroelastic waves. Theor. Appl. Mech. Lett. 12, 100315.

Wang, Z., Wang, Z., Yuan, C., 2022. Oceanic internal solitary waves in three-layer fluids of great depth. Acta Mech. Sinica 38, 321473.
Whitham, G., 1974. Linear and Nonlinear Waves. John Wiley & Sons. Inc. New York.
Whitham, G.B., Lighthill, M.J., 1967. Variational methods and applications to water waves. Proc. R. Soc. Lond. A 299, 6–25.
Yuan, C., Grimshaw, R., Johnson, E., Chen, X., 2018. The propagation of internal solitary waves over variable topography in a horizontally two-dimensional framework. J. Phys. Oceanogr. 48 (2), 283–300.
Yuan, C., Wang, Z., 2022. On diffraction and oblique interactions of horizontally two-dimensional internal solitary waves. J. Fluid Mech. 936, A20.
Yuan, C., Wang, Z., Chen, X., 2020. The derivation of an isotropic model for internal waves and its application to wave generation. Ocean Model. 153, 101663.
Zhou, X., Grimshaw, R., 1989. The effect of variable currents on internal solitary waves. Dyn. Atmos. Oceans 14, 17–39.
Ziegenbein, J., 1969. Short internal waves in the strait of gibraltar. Deep Sea Res. Oceanogr. Abstr. 16 (5), 479–487.
Ziegenbein, J., 1970. Spatial observations of short internal waves in the strait of gibraltar. Deep Sea Res. Oceanogr. Abstr. 17 (5), 867–875.